LETTERS

Shaping mobile belts by small-scale convection

Claudio Faccenna[1,2] & Thorsten W. Becker[3]

Mobile belts are long-lived deformation zones composed of an ensemble of crustal fragments, distributed over hundreds of kilometres inside continental convergent margins[1,2]. The Mediterranean represents a remarkable example of this tectonic setting[3]: the region hosts a diffuse boundary between the Nubia and Eurasia plates comprised of a mosaic of microplates that move and deform independently from the overall plate convergence[4]. Surface expressions of Mediterranean tectonics include deep, subsiding backarc basins, intraplate plateaux and uplifting orogenic belts. Although the kinematics of the area are now fairly well defined, the dynamical origins of many of these active features are controversial and usually attributed to crustal and lithospheric interactions. However, the effects of mantle convection, well established for continental interiors[5–7], should be particularly relevant in a mobile belt, and modelling may constrain important parameters such as slab coherence and lithospheric strength. Here we compute global mantle flow on the basis of recent, high-resolution seismic tomography to investigate the role of buoyancy-driven and plate-motion-induced mantle circulation for the Mediterranean. We show that mantle flow provides an explanation for much of the observed dynamic topography and microplate motion in the region. More generally, vigorous small-scale convection in the uppermost mantle may also underpin other complex mobile belts such as the North American Cordillera or the Himalayan–Tibetan collision zone.

Deep to intermediate seismicity in the Mediterranean is restricted to the Hellenic and Calabria Wadati–Benioff zones and locally beneath the Alboran region[8], although fast seismic velocity anomalies[9–11] run discontinuously all along the alpine Tethyan suture, from North Africa to the Calabria–Apennines, twisting beneath the Alps, the Carpathians–Dinarides–Hellenides, and further to the east joining the Bitlis–Zagros zone. Most of these fast anomalies are not connected to the surface. This indicates that the once almost-continuous subduction zone is now fragmented, owing to the entrance at the trench of small continental fragments under the slow ($\sim$1 cm yr^{-1}) Nubia–Eurasia convergence[9,12]. Eventually, this process generates new plate boundaries, producing the complex pattern observed today (Fig. 1). For example, the collision along the Zagros–Bitlis belt induced the westward motion of Anatolia and the formation of the North Anatolian fault[3]. Soon after, Aegea separated from Anatolia, moving southward towards the Hellenic trench. To the west, the arrival of the African continent at the trench locked the Calabria–North Africa subduction zone, generating a new convergent boundary along the pre-existing passive African margin (Fig. 1). Although the overall kinematics of these processes are now fairly well established, the dynamics are still debated. Proposed models include gravitational potential energy contrasts within the crust[13], plate (edge force) interactions, subduction[12] and large-scale mantle flow[14].

To quantify the contribution of mantle circulation to surface tectonics, we compute instantaneous, three-dimensional spherical mantle flow driven by temperature (density) anomalies as inferred from seismic tomography, assuming that velocity anomalies are simply related to temperature[5]. Flow produced by density anomalies within the mantle stresses the lithospheric plates and produces both horizontal and vertical motions. For the Mediterranean case, we leave the Adria and Anatolia–Aegea microplates free of shear stress (white arrows in Fig. 2a) so that they can be pulled by the mantle, while the lithospheres of Nubia, Eurasia and Arabia are prescribed to move with NUVEL-1A model velocities[15] (grey vectors, applied only at the surface), leaving the underlying mantle flowing freely. The normal stresses generated by viscous flow at the surface are used to infer the equivalent 'dynamic' topography. Assuming no erosion, the dynamic topography can be compared to the 'residual' topography (Fig. 1b), calculated by removing the isostatic adjustment from the topography[6,7].

Figure 2 shows mantle velocities for the reference model in a Eurasia fixed reference frame. At shallow depths ($\sim$100–300 km, Fig. 2c), the regional flow field shows a large-scale, toroidal current from Arabia to the western Mediterranean perturbed by density anomalies associated with the Hellenic slab, Calabrian slab and the western Alpine slab. Subduction zones generate downward pull towards the inner portion of their respective arcs, where deep mantle slabs accumulate (Fig. 2c), ponding in the transition zone (Fig. 2e). Downward flow is accompanied by an upwelling return flow between slabs and at their edges. In cross-section, this pattern corresponds to

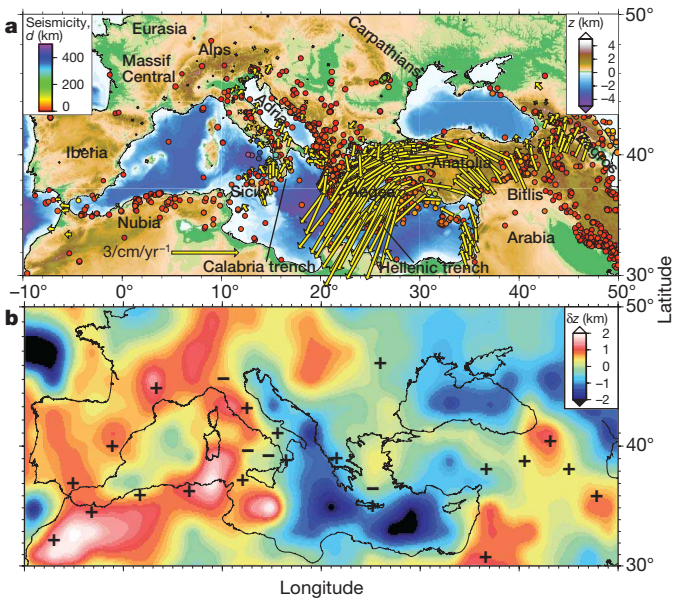

Figure 1 | Topography and deformation indicators for the Mediterranean. **a**, GPS measurements (yellow arrows, Eurasia fixed reference frame[24]) and seismicity (dots, colour-coded by depth) with magnitude $M > 5$ (ref. 8), colour-coded by depth. *z*, Elevation. **b**, Residual topography relative to a regional mean, estimated by correcting for isostatic adjustment using the CRUST2.0 model[30]; with plus and minus symbols showing uplift and subsidence, respectively (see text for references).

[1]Dipartimento Scienze Geologiche, University Roma TRE, 00146 Rome Italy. [2]Consiglio Nazionale Ricerche—IGAG 00016, Rome, Italy. [3]Department of Earth Sciences, University of Southern California, Los Angeles, California 90089-0740, USA.

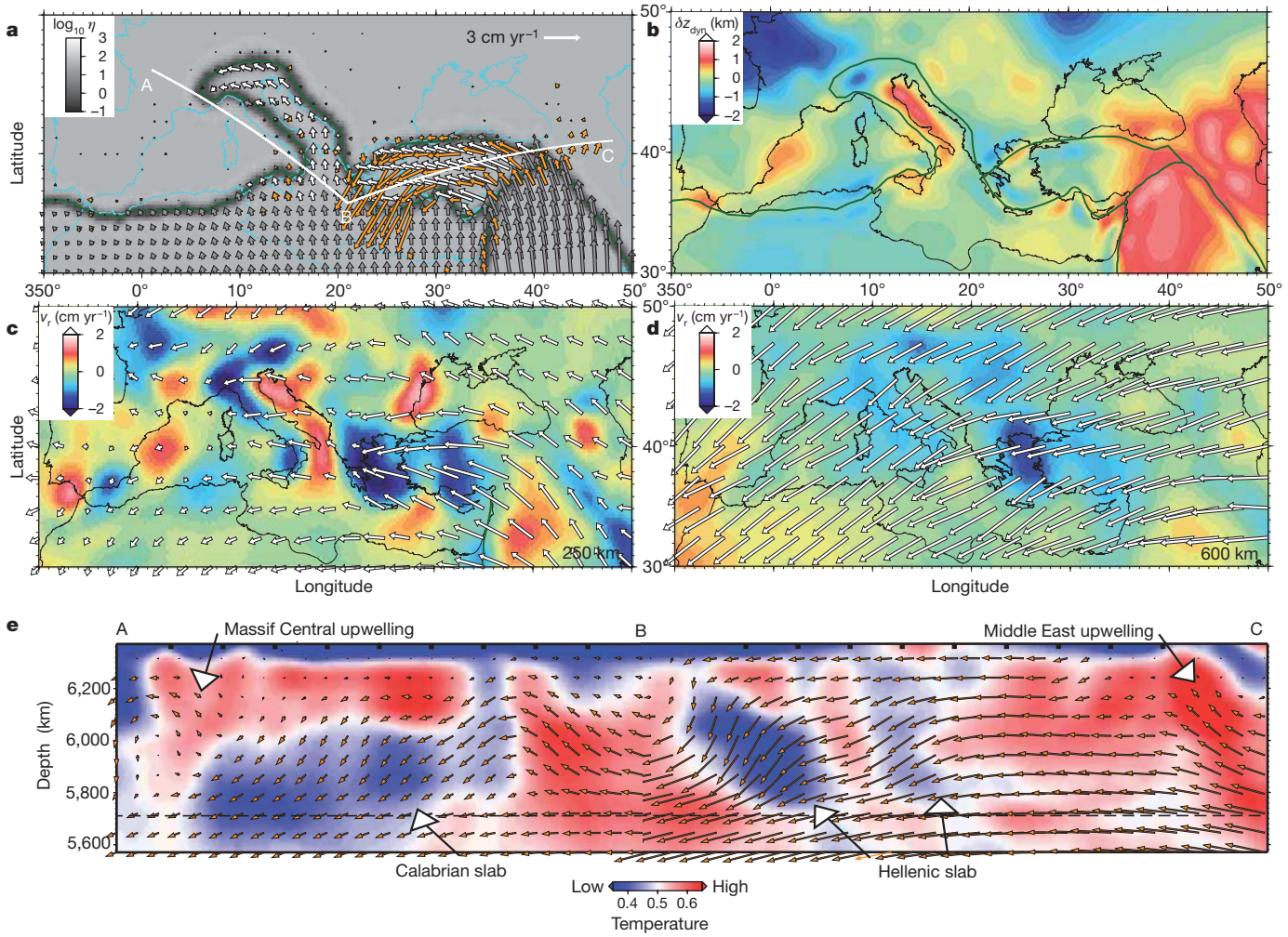

Figure 2 | Reference flow model for the Mediterranean region. The model is based on the tomography model of ref. 11. **a**, Layer viscosity η and predicted surface velocities of Adria and Anatolia–Aegea (white vectors). Geodetic velocities (orange vectors) and prescribed velocities (grey vectors, from NUVEL-1A) are in the Eurasia fixed reference frame. Plate boundaries are treated as weak narrow belts, with a simplified geometry merging the eastern Alps with the Dinarides. **b**, Predicted dynamic topography (z_{dyn} is dynamic elevation, boundary in green). **c**, **d**, Horizontal (white vectors) and vertical flow (background colour shading) field at 250 km (**c**) and 600 km depth (**d**). **e**, Cross-sections from Massif Central to Calabria and to Anatolia (marked in **a**), with temperature (normalized by a reference temperature) in the background.

an undulated flow confined to the uppermost portion of the mantle (Fig. 2e). Details of the flow and topography depend upon assumptions such as the seismic velocity anomaly to density scaling, and the coupling of the slab to the plate, but the overall patterns are insensitive to assumptions about rheology (Supplementary Fig. 3), or the adopted tomographic model (Supplementary Fig. 4). Figure 2e shows that flow is at an angle to the ~25–30 mm yr^{-1} retreating Hellenic slab, but parallel down-dip to the stationary Calabria slab. This agrees with theoretical expectations of slab-induced flow[16], indicating differences in slab force transmission. The subduction-related downward flow induces pronounced (~1 km) negative dynamic topography within the non-compensated[17], dynamically subsiding, southern Tyrrhenian and Cretean sea backarc basins[18].

The pull exerted by the retreating Hellenic slab, coupled with an upwelling in the Middle East, helps propel Anatolia westward (Fig. 2a)—why it moved westward has been the subject of controversy over the past few decades[4]. Our model shows a reasonable fit with geodetic data, indicating that Anatolia's motion is about equally driven by slab anomalies (Fig. 3a), which leads to large-scale toroidal flow at depth, and by the indenting Arabia plate (Supplementary Fig. 3a), which leads to lithospheric push. The Bitlis suture in eastern Anatolia acts as a more efficient strain guide when the plates are coupled (that is, no weak zone on the plate boundary; Fig. 3b). The mantle upwelling beneath the Near East is a particularly pronounced feature, extending from north Arabia to eastern Anatolia and the Caucasus. A comparison of dynamic and residual topography indicates that this upwelling is responsible for the uplift and elevation of the whole region, notably of the Anatolia high plateau, and also for intraplate volcanism[19] (Fig. 1b). Our results indicate that this upward flow is probably rooted in the transition zone (Fig. 2e), and could be triggered by the subducted Hellenic (Tethyan) slab. However, its far-field linkage with the large-scale upwelling over the east Africa–southeast Arabia plate cannot be ruled out[7].

Our model fails to reproduce the fast southward motion of Aegea with respect to Anatolia, because the mantle anomaly is positioned mostly beneath the western side of the Hellenic trench (Supplementary Fig. 1a), such that little southward pull is induced. This may be due partially to a simplified treatment of the trench without faults, and rheologically more realistic cases with stiff slabs and resulting asymmetric force transmission, or density anomalies inferred from slab seismicity slightly improves our solution (Supplementary Fig. 3d). This indicates that the motion of Aegea is probably dominated by crustal gravitational potential energy variations not included here. Indeed, the crustal column of the Aegean is probably thickened and weakened enough to be prone to extension towards the Hellenic trench[13].

Between the Calabria–Apennines and the Hellenides–Dinarides subduction zones, the mantle is upwelling, reflecting both passive

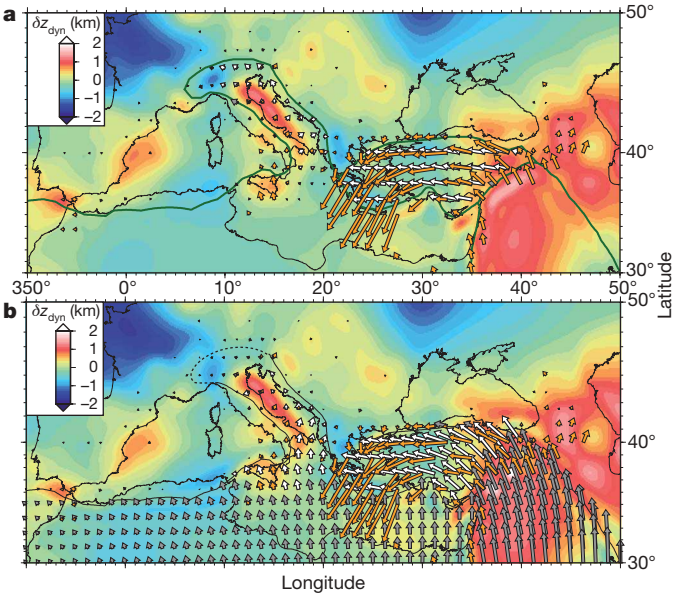

Figure 3 | Additional flow models for the Mediterranean. Surface velocities (as in Fig. 2a) are superimposed on dynamic topography (as in Fig. 2b). **a**, Flow (white vectors) generated by density anomalies only (that is, surface held fixed outside the microplates). **b**, Reference model with Bitlis and Alps collisional zones coupled (weak zones removed within dashed regions). Geodetic velocities (orange vectors) and prescribed velocities (grey vectors, from NUVEL-1A) are in the Eurasia fixed reference frame.

return flow squeezed by two opposite-facing retreating slabs, and active flow due to shallow-mantle, low-velocity anomalies (Fig. 2). The details of the dynamic topography depend on the adopted tomographic model (compare Fig. 2b and Supplementary Fig. 4a, e), but the general features are robust and explain the uplift observed over southern Italy[20] and intraplate rifting and volcanism in the Sicily channel[21]. Free air gravity analysis[22] and mantle flow computations[23] extend this dynamic signature also into the northern Apennines. The opposite-facing slabs anchor the small Adria plate. As inferred from geodesy, Adria indeed moves slowly and its Euler vector is not coherent with the motion of Nubia[24,25]. We found that Adria kinematics can be better fitted by adding the eastward pull of the Hellenic slab to the northward Nubia motion (compare Figs 2a and 3a). This provides an alternative explanation to the in-plane block-interaction model[25]. Geodetic data show that the northern portion of Adria is moving north-northeast (Fig. 1), revealing a recent change from the westward motion deduced by fault kinematics in the southern Alps. Our results show that this earlier motion could be related to the pull exerted by the mantle beneath the Alps (Fig. 3a), whereas the present-day motion can be reproduced by coupling the plate boundary beneath the Alps (removal of the northern weak zone; Fig. 3b).

Just as in the Middle East, a vigorous upwelling is present in the western Mediterranean, from southern Iberia to the Massif Central. Here, it is apparent that this flow is connected to the western Mediterranean high-velocity anomaly, forming an upwelling–downwelling cell restricted to the uppermost mantle (Fig. 2c and e). Residual topography (Fig. 1b) matches these non-compensated features beneath eastern Iberia, suggesting that the origin of Quaternary alkaline volcanism, and of the uplift of the ~850-m-high plateau-like *mesetas*[26] is related to mantle dynamics. The Massif Central represents a similar, but more focused, feature in which the long-lived alkaline volcanic province[21] has been previously related to a mantle plume. In contrast, we suggest that volcanism can be caused by decompression melting related to a large-scale return flow at the trailing edge of the western Mediterranean slab (Fig. 2e). SKS wave splitting anisotropy supports this hypothesis, because splitting directions beneath the Massif Central are parallel to the flow generated by the retreating Calabria slab[27].

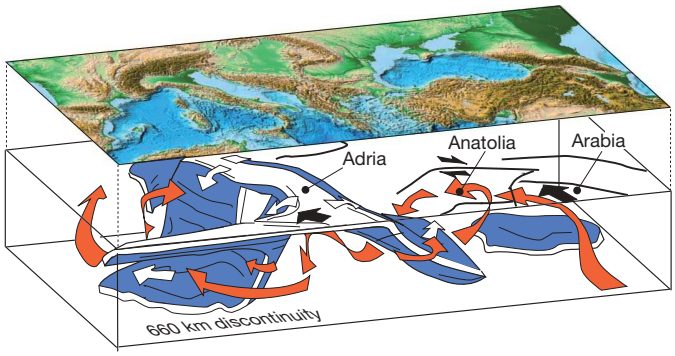

Figure 4 | Cartoon illustrating the architecture of the subduction zones and the related pattern of mantle convection in the Mediterranean region. Vigorous convection (red arrows) is mainly confined to the uppermost portion of the upper mantle and related to subduction (white arrows) within the Africa–Eurasia convergence (black arrows) . We note also the large-scale toroidal flow beneath the Middle East.

To isolate the contribution of mantle flow, we simplified our model by excluding crustal effects such as gravitational potential energy contributions. Nevertheless, based on the fairly high-resolution (down to ~100 km) tomography beneath the Mediterranean upper mantle[9–11], we are able to analyse the signal generated by regional mantle anomalies within a complex tectonic region. Mantle circulation induced by slab fragments within a mobile zone seems to be more important than previously thought, and generates vigorous upwellings even far from the subduction zone (Fig. 4). We can contrast those short-wavelength currents originating between the base of the lithosphere and the transition zone with those associated with the longer-wavelength, subdued mantle anomalies below ~400 km. In the Mediterranean region, irrespective of the adopted rheological stratification, such small-scale convection appears to be dominant in the origin and mobility of crustal fragments and for the large uncompensated topography (Fig. 4).

This multi-scale pattern of convection may well apply to other mobile belts such as the North American Cordillera or the Himalayan–Tibetan belt. Also in these regions, discontinuously subducting slab segments could excite vigorous flow confined to the uppermost mantle—which may explain the lateral escape of crustal fragments and produce pronounced topographic signals. We speculate that this vigorous small-scale convection could be the ultimate cause of the distribution of convergent deformation inside continental domains.

METHODS SUMMARY

To model mantle flow, we solve the equations for instantaneous fluid circulation using the global, finite-element code CitcomS[28]. Mechanical boundary conditions are of mixed type: although the velocities of large plates are prescribed at the surface, the regions shown by white vectors in Fig. 2a are left free of shear stress (that is, free slip, allowing for dynamically consistent regional plate motions). Internally, flow is additionally driven by density anomalies, which are inferred by scaling velocity anomalies from seismic tomography to temperature[29]. Results shown here are based on a mesh resolution of ~20 km, and tests indicate that overall model uncertainties are mainly due to imperfect knowledge of input models, such as tomography, and are not due to computational limitations.

Our reference density structure is based on recent, global *P*-wave tomography[11], which provides, in general, high-resolution (down to ~100 km) images of subduction zones. The rheology of the mantle is Newtonian viscous and most models have only radial-viscosity variations besides weak zones confined to the lithosphere (down to 100 km depth), have 100 km width, and a viscosity reduction to 0.01 of the ambient viscosity. The reference, radial-viscosity structure is 5×10^{22} Pa s in the lithosphere, 10^{21} Pa s from 100–660 km, and 5×10^{22} Pa s in the lower mantle. Tests using different rheology and input model choices are described in the Supplementary Information.

Received 11 October 2009; accepted 26 March 2010.

1. Molnar, P. Continental tectonics in the aftermath of plate tectonics. *Nature* **335**, 131–137 (1988).

2. Hyndman, R. D., Currie, C. A. & Mazzotti, S. Subduction zone backarcs, mobile belts, and orogenic heat. *GSA Today* **15,** doi:10:1130/1052–5173(2005)015 (2005).
3. McKenzie, D. P. Active tectonics of the Mediterranean region. *Geophys. J. R. Astron. Soc.* **30,** 109–185 (1972).
4. Reilinger, R. *et al.* GPS constraints on continental deformation in the Africa-Arabia-Eurasia continental collision zone and implications for the dynamics of plate interactions. *J. Geophys. Res.* **111,** B05411, doi:10.1029/2005JB004051 (2006).
5. Lithgow-Bertelloni, C. & Silver, P. G. Dynamic topography, plate driving forces and the African superswell. *Nature* **395,** 269–272 (1998).
6. Gurnis, M. Sculpting the earth from inside out. *Sci. Am.* **284,** 40–47 (2001).
7. Daradich, A., Mitrovica, J. X., Pysklywec, R. N., Willet, S. D. & Forte, A. M. Mantle flow, dynamic topography, and rift-flank uplift of Arabia. *Geology* **31,** 901–904 (2003).
8. Engdahl, E. R., van der Hilst, R. D. & Buland, R. Global teleseismic earthquake relocation with improved travel times and procedures for depth determination. *Bull. Seismol. Soc. Am.* **88,** 722–743 (1998).
9. Wortel, M. J. R. & Spakman, W. Subduction and slab detachment in the Mediterranean-Carpathian region. *Science* **290,** 1910–1917 (2000).
10. Piromallo, C. & Morelli, A. P-wave tomography of the mantle under the Alpine–Mediterranean area. *J. Geophys. Res.* **108,** doi:10.1029/2002JB001757 (2003).
11. Li, C., van der Hilst, R. D., Engdahl, E. R. & Burdick, S. A new global model for P wave speed variations in Earth's mantle. *Geochem. Geophys. Geosyst.* **9,** Q05018, doi:10.1029/2007GC001806 (2008).
12. Royden, L. H. Evolution of retreating subduction boundaries formed during continental collision. *Tectonics* **12,** 629–638 (1993).
13. Gautier, P. *et al.* Timing, kinematics and cause of Aegean extension: a scenario based on a comparison with simple analogue experiments. *Tectonophysics* **315,** 31–72 (1999).
14. Doglioni, C. A proposal for the kinematic modelling of the W-dipping subductions—possible applications to the Tyrrhenian-Apennines system. *Terra Nova* **4,** 423–434 (1991).
15. DeMets, C., Gordon, R. G., Argus, D. F. & Stein, S. Effect of recent revisions to the geomagnetic reversal time scale on estimates of current plate motions. *Geophys. Res. Lett.* **21,** 2191–2194 (1994).
16. Garfunkel, Z., Anderson, C. A. & Schubert, G. Mantle circulation and the lateral migration of subducted slabs. *J. Geophys. Res.* **91,** 7205–7223 (1986).
17. Seber, D. *et al.* Crustal model for the Middle East and North Africa region: implications for the isostatic compensation mechanism. *Geophys. J. Int.* **147,** 630–638 (2001).
18. Husson, L. Dynamic topography above retreating subduction zones. *Geology* **34,** 741–744 (2006).
19. Sengor, A. M., Ozeren, C. S., Genç, T. & Zor, E. East Anatolia high plateau as a mantle supported, north–south shortened domal structure. *Geophys. Res. Lett.* **30,** 8045–8049 (2003).
20. Ferranti, L. *et al.* Markers of the last interglacial sea level highstand along the coast of Italy: tectonic implications. *Quat. Int.* **145–146,** 30–54 (2006).
21. Lustrino, M. & Wilson, M. The circum-Mediterranean anorogenic Cenozoic igneous province. *Earth Sci. Rev.* **81,** 1–65 (2007).
22. D'Agostino, N. & McKenzie, D. Convective support of long wavelength topography in the Apennines (Italy). *Terra Nova* **11,** 234–238 (1999).
23. Shaw, M. & Pysklywec, R. Anomalous uplift of the Apennines and subsidence of the Adriatic: The result of active mantle flow? *Geophys. Res. Lett.* **34,** L04311, doi:10.1029/2006GL028337 (2007).
24. Serpelloni, E. *et al.* Kinematics of the Western Africa–Eurasia plate boundary from focal mechanisms and GPS data. *Geophys. J. Int.* **169,** 1180–1200 (2007).
25. D'Agostino, N. *et al.* Active tectonics of the Adriatic region from GPS and earthquake slip vectors. *J. Geophys. Res.* **113,** B12413, doi:10.1029/2008JB005860 (2008).
26. Casas-Sainz, A. M. & de Vicente, G. On the tectonic origin of Iberian topography. *Tectonophysics* **474,** 214–235 (2009).
27. Lucente, F. P., Margheriti, L., Piromallo, C. & Barruol, G. Seismic anisotropy reveals the long route of the slab through the western-central Mediterranean mantle. *Earth Planet. Sci. Lett.* **241,** 517–529 (2006).
28. Zhong, S., Zuber, M. T., Moresi, L. & Gurnis, M. Role of temperature-dependent viscosity and surface plates in spherical shell models of mantle convection. *J. Geophys. Res.* **105,** 11063–11082 (2000).
29. Simmons, N. A., Forte, A. M. & Grand, S. P. Joint seismic, geodynamic and mineral physical constraints on three-dimensional mantle heterogeneity: Implications for the relative importance of thermal versus compositional heterogeneity. *Geophys. J. Int.* **177,** 1284–1304 (2009).
30. Bassin, C., Laske, G. & Masters, G. The current limits of resolution for surface wave tomography in North America. *Eos* 81, abstr. F897 (2000).

Supplementary Information is linked to the online version of the paper at www.nature.com/nature.

Acknowledgements C.F. thanks the University of Southern California (USC) and the Consiglio Nazionale Ricerche for supporting his visit at USC. This work has been financially supported by TOPOEUROPE and MEDUSA (NSF-EAR 0451952), computations were performed on USC's High Performance Computing Center, and we thank the Computational Infrastructure for Geodynamics and the seismologists who shared their tomographic models in electronic form. C.F. thanks R. Funiciello for his support and suggestions.

Author Contributions T.W.B. performed numerical modelling, C.F. designed the modelling strategy. Both authors contributed equally to interpreting and analysing the data and to writing the paper.

Author Information Reprints and permissions information is available at www.nature.com/reprints. The authors declare no competing financial interests. Readers are welcome to comment on the online version of this article at www.nature.com/nature. Correspondence and requests for materials should be addressed to C.F. (faccenna@uniroma3.it).

SUPPLEMENTARY INFORMATION

The major uncertainties in our model predictions arise from the input parameters, which include mantle density models (i.e. seismic tomography and choices about scaling velocities to temperature), crustal models, the kinematic boundary conditions (surface velocities), and assumptions about mantle rheology. We here present a few of the additional computations we performed to establish that the model results shown in our paper are robust with respect to these choices.

Our reference mantle density model (model A) is based on the global *P* wave model from the MIT group (ref. 11, Fig. S1a) which provides, generally speaking, well resolved images of subduction zones (down to ~100 km scales) while imaging the oceanic upper mantle (e.g. Pacific domain) less well because of ray path incidence. To test alternative tomography structures, we first use the high resolution *P* model by ref. 10 for the Mediterranean which employs both regional and teleseismic arrivals. This regional model was embedded in the global *S* wave model by ref. 29 by replacing nodes within the region by the regional *P* results, scaled up by a factor of two (model B, Fig. S1b). The second alternative, model C, is based on the global, upper mantle *SV* model of ref. S1, augmented by an *S* composite model (SMEAN of ref. S2) in the lower mantle below 660 km (model C, Fig. S1c).

Residual topography as inferred from crustal models was estimated by correcting the observed topography for isostatic adjustment given the density structure of CRUST2.0[30] for results presented in the main text. Since CRUST2.0 is fairly low resolution, we also consider the EuCRUST7 model[S3] which has, however, no densities given. We use the CRUST2.0 averages of 2330 kg/m^3 for sediments, and 3086 kg/m^3 for a single crustal layer for consistency. Fig. S2 shows the residual topography using this crustal model and can be

compared with Fig. 1b. Figure S3 shows dynamic topography and crustal fragment motions for several exploratory models, using the density model A as used in the main text for reference. Fig. S3a is for a model without any density anomalies, showing which components of the microplate motions are associated with purely large-scale, plate motion induced currents. Our reference, radial viscosity structure is $5 \cdot 10^{22}$ Pas in the lithosphere, 10^{21} Pas from 100-660 km, and $5 \cdot 10^{22}$ Pas in the lower mantle; a model with a lower viscosity asthenosphere (viscosity reduced by a factor of 0.1 between 100 and 300 km) is shown as Fig. S3b; mantle flow effects are still significant. Temperature-dependent viscosity with variations of ~four orders of magnitude laterally within the upper mantle (Fig. S3c) also do not produce a strongly different velocity field or dynamic topography from the reference model. Fig. S3d shows model predictions for a density structure that only includes anomalies due to slabs in regions of seismicity in Wadati-Benioff zones, plus an additional shear zone between the Agean and Anatolian plate. These modifications improve the fit of the Agean segment motion to geodetic velocities somewhat, though the southwestward motions are still under-predicted. Fig. S3e combines the temperature-dependent viscosity model of Fig. S3c with the additional effect of stiff keels with a factor of 500 increase of viscosity underneath cratonic regions of ref. S5; model predictions show somewhat subdued dynamic topography but major features are unchanged.

Velocities for the reference models are prescribed in an Eurasia fixed reference frame based on NUVEL-1A[15]. While NUVEL-1A locally differs from the geodetically observed, approximate rigid plate motions (Fig. 1), it has the advantage of being global in scope and independent from the geodetic data. Using rotation pole of ref. 24 for Nubia instead of NUVEL-1A for modelling rotates boundary velocities as expected, but does not affect our

conclusions otherwise (Fig. S3f). While there are important differences in the global plate driving forces predicted from *S* and *P* tomography (e.g. ref. S4), these differences are less relevant for our confined study region, and overall predictions using all three models, e.g. in terms of dynamic topography, are indeed quite similar (Fig. S4). In particular, we note that the velocity field obtained in the Model C based on global SV wave model[S1] is also similar to the reference model, matching better the Aegean motion, but probably overestimating the positive dynamic topography (Fig. S4e).

Supplementary References

S1. Lebedev, S., Van der Hilst, R.D. Global upper-mantle tomography with the automated multimode inversion of surface and S-wave forms. *Geophys. J. Int.*, 173, 505-518 (2008).

S2. Becker, T. W. and Boschi, L. A comparison of tomographic and geodynamic mantle models. *Geochem., Geophys., Geosyst.*, 3(1), 1003, doi:10.1029/2001GC000168 (2002).

S3. Tesauro, M., Kaban, M. K. & Cloetingh, S. A. P. L. EuCRUST -07: A new reference model for the European crust. *Geophys. Res. Letters* 35, L05313, doi:10.1029/2007GL032244 (2008).

S4. Becker, T. W. and O'Connell, R. J. Predicting plate velocities with mantle circulation models. *Geochem., Geophys., Geosys.*, 2(12), doi:10.1029/2001GC000171 (2001).

S5. Nataf, H.-C. and Ricard, Y. 3SMAC: an *a priori* tomographic model of the upper mantle based on geophysical modeling. *Phys. Earth Planet. Int.,* 95, 101-122 (1996).

Supplementary Figures

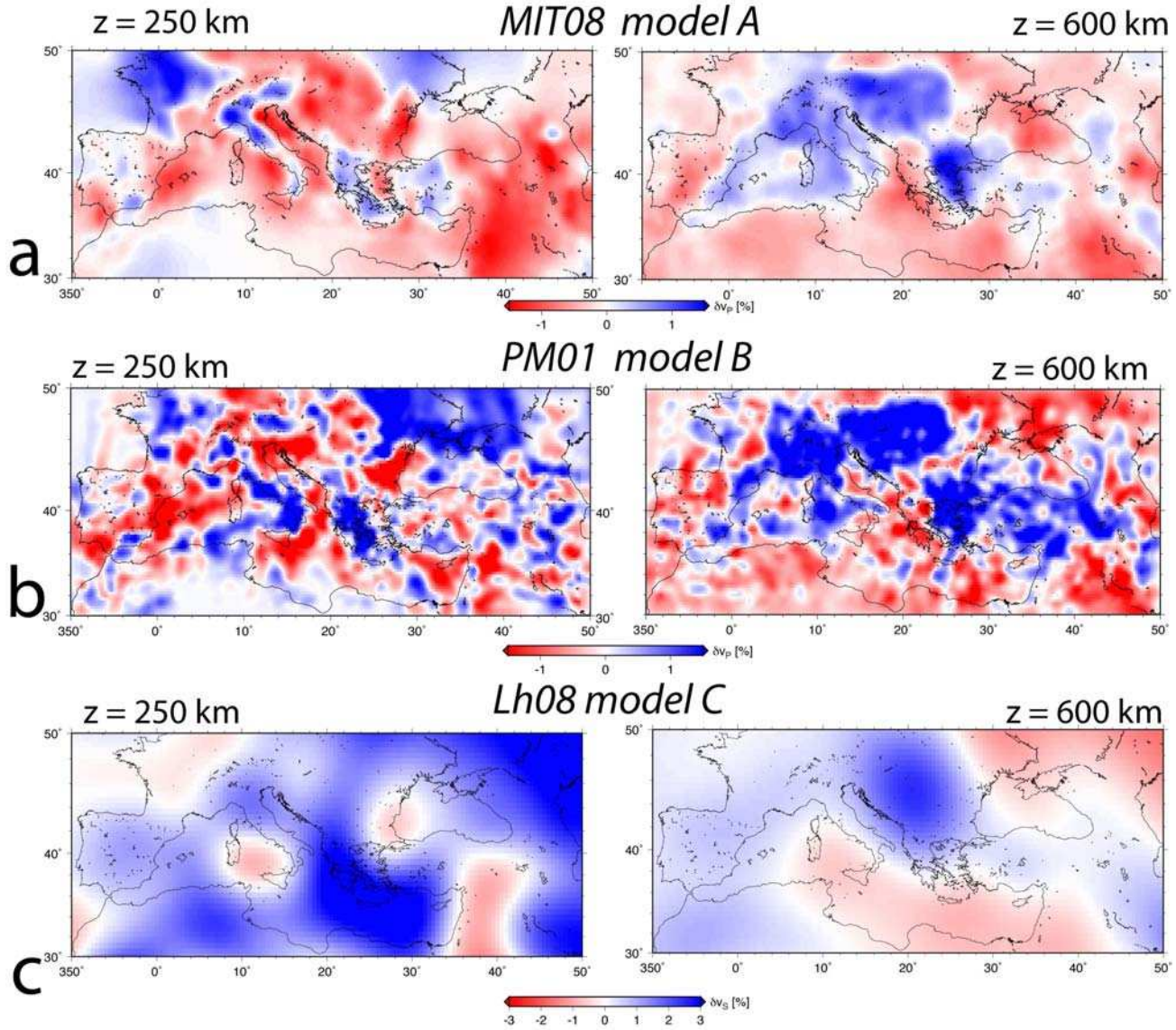

Supplementary Figure S1. Comparison of velocity anomaly maps of tomographic models used. a) Reference model A, *MIT08* [11], at 250 km and 600 km depth; b) Tomography maps of model B, the merged PM01[10] /TX2008[29] model at 250 km and 600 km depth; c) Maps of model C, the *SV* wave study LH08 of ref. S1 at 250 km and 600 km depth.

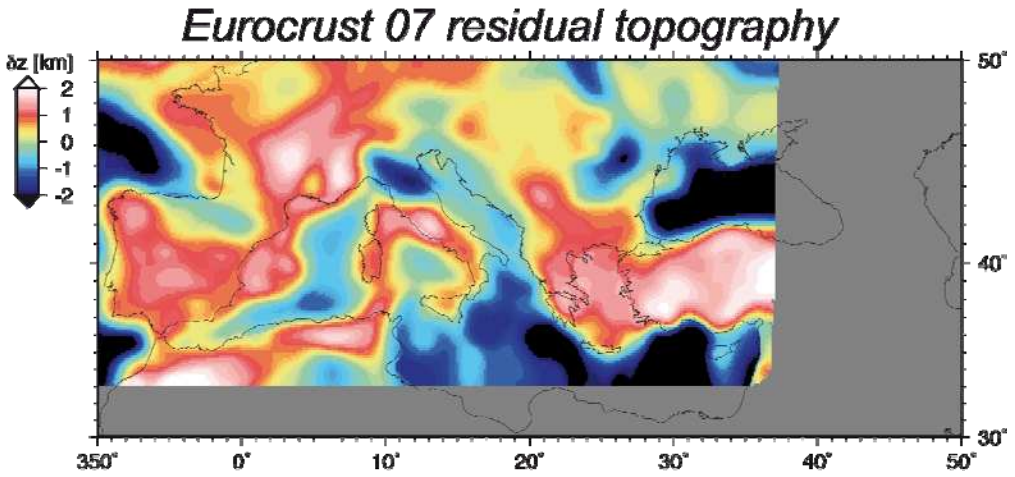

Supplementary Figure S2. Alternative residual topography estimated by correcting the Eurocrust07 crustal thickness model[S3] for isostasy using mean CRUST2.0 densities for a sediment and crust layer.

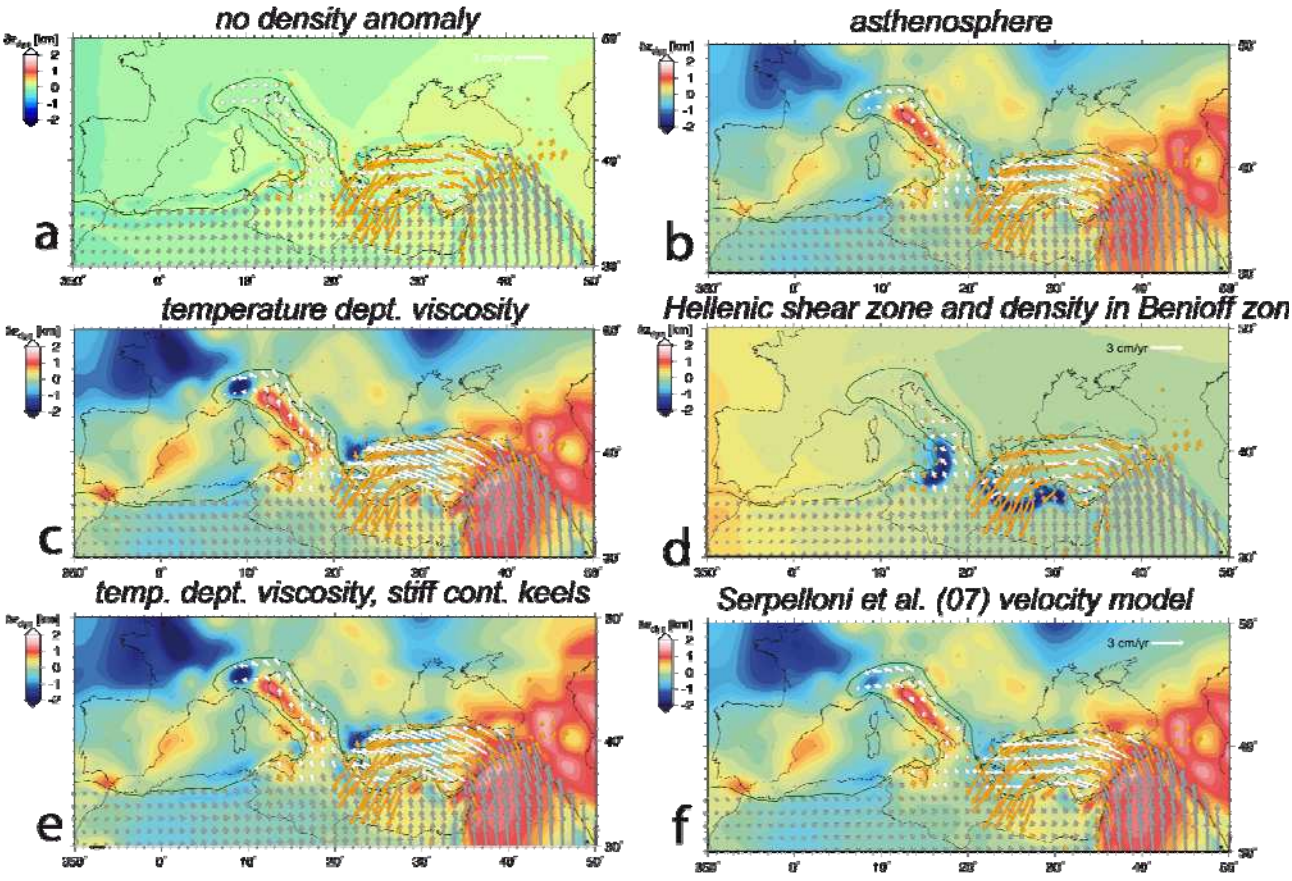

Supplementary Figure S3. Additional flow solution as variations of model A. a) Flow generated only by plate interactions (i.e. no density anomalies); b) flow with asthenospheric layer where the viscosity was reduced by a factor of ten from the reference between 100 and 300 km depth; c) flow generated by temperature-dependent viscosity, corresponding to four orders of magnitude variation laterally within the upper mantle; d) flow generated by density anomalies in Wadati-Benioff zones only, and using an additional plate boundary in western Anatolia separating Anatolia from an Aegean microplate (additional weak zone in dashed region); e) temperature dependent viscosity as in c) plus additional stiff keels beneath cratonic regions (factor 500 stiffer than ambient); f) flow generated by prescribing the velocity field of Nubia with respect to Eurasia based on the geodetic pole of ref. 24.

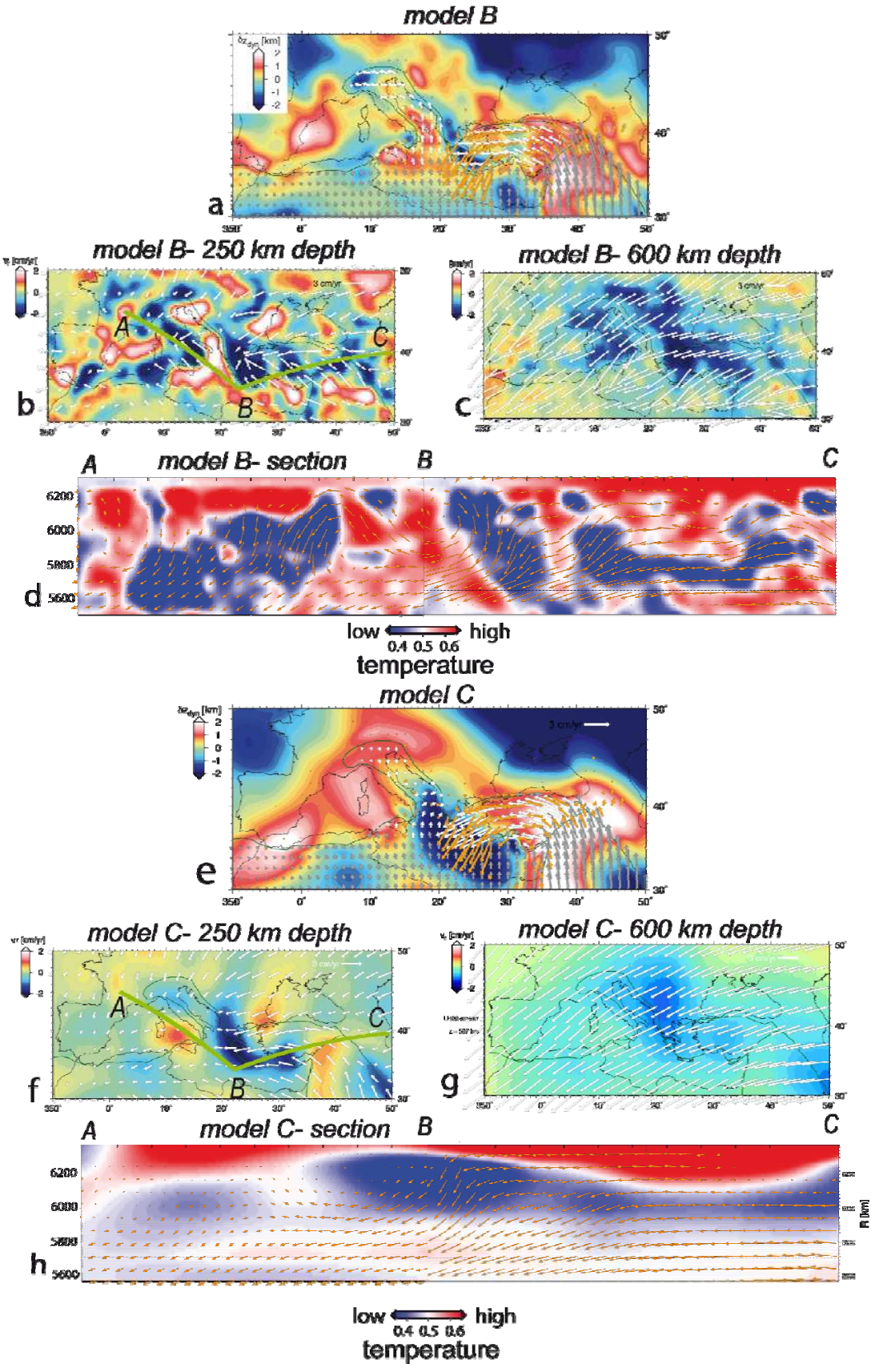
model B
a
model B- 250 km depth
b
A
B
C
model B- 600 km depth
c
model B- section
A
B
C
6200
6000
5800
5600
d
low
high
0.4 0.5 0.6
temperature
model C
e
model C- 250 km depth
f
A
B
C
model C- 600 km depth
g
model C- section
A
B
C
6200
6000
5800
5600
h
low
high
0.4 0.5 0.6
temperature

Supplementary Figure S4. Additional flow solution based on different tomography models. a) Density anomalies based on merged regional tomography of ref. 10 with global tomography of ref. 30 (model B); b) Horizontal and vertical flow field for model B at 250 km, and c) 600 km depth. d) Section of model B running from Massif Central to Calabria and then to Anatolia, plotted on top of inferred temperature anomalies from the tomography model. e) Model C: flow model generated by SV wave tomography of ref. S1. f) Horizontal and vertical flow field for model C at 250 km and g) 600 km depth. h) Section of model C running from Massif Central to Calabria and then to Anatolia, plotted on top of inferred temperature anomalies from the tomography model.